DOI: 10.32615/ps.2020.015 PHOTOSYNTHETICA 58 (SI): 671-681, 2020

Special issue in honour of Prof. Reto J. Strasser

Phosphorus deficiency affects the I-step of chlorophyll *a* fluorescence induction curve of radish

M.D. CETNER[*,+], H.M. KALAJI[*], W. BORUCKI[**], and K. KOWALCZYK[***]

Department of Plant Physiology, Institute of Biology, Warsaw University of Life Sciences WULS-SGGW, 159 Nowoursynowska Street, 02-776 Warsaw, Poland[*]
Department of Botany, Institute of Biology, Warsaw University of Life Sciences WULS-SGGW, 159 Nowoursynowska Street, 02-776 Warsaw, Poland[**]
Department of Vegetable and Medicinal Plants, Institute of Horticulture Sciences, Warsaw University of Life Sciences WULS-SGGW, 166 Nowoursynowska Street, 02-787 Warsaw, Poland[***]

Abstract

Phosphorus (P) is an essential nutrient for plant development and its fertilisation efficiency is an important issue in agriculture. Difficulties in diagnosing P deficiency in plants have created a demand for a quick and noninvasive method/tool for assessing plant P status on-site. It has been well documented that chlorophyll fluorescence measurement is a very useful and sensitive tool for screening nutrients deficiency in plants. Although impact of P deficiency on photosynthesis process has been widely examined, its effect/s on photosynthetic electron transport between the two photosystems is still not clear. In this work, we studied the response of radish plants to P deficiency throughout stress conditions and recovery period. Leaf phosphorus content, growth rate, and photosynthetic activity and efficiency were monitored. Under P deficiency, a decrease in all of these physiological features was observed. Moreover, some changes in chloroplast structure were explored, including a reduction in chloroplast grana amount and loose arrangement. Additionally, the I-step disappeared from chlorophyll fluorescence induction curves. This can be linked to the inactivation of PSI and suppression of the cyclic phosphorylation. The observed decreases in quantum yield and the efficiency of electron transport chain in P-deficient plants could be due to downregulation mechanisms in the photosynthetic apparatus. However, both the inhibition of net photosynthetic rate, as well as the severe effect on the I-step were reversible when plants were resupplied with phosphorus. Loss of I-step can be used as a specific bioindicator for early detection of phosphorus deficiency in radish plants.

Additional key words: gas exchange; hydroponics; JIP-test; phosphate.

Introduction

Phosphorus (P) is one of the essential nutrients that determines plant growth and productivity. Its deficiency is worldwide common, covers an area of over 2 billion ha (Fairhurst *et al*. 1999), and is known to reduce crop yield severely (Malhotra *et al.* 2018). On other hand, in some parts of the world P fertilisers are overused causing severe eutrophication (MacDonald *et al.* 2011). Thus, considering that phosphate rock, the main source of phosphate

Received 15 November 2019, *accepted* 13 February 2020.
[+]Corresponding author; e-mail: magdalena.cetner@gmail.com
Abbreviations: cyt b_6f – cytochrome b_6f complex; DAT – days after treatment; ET_0/RC – electron transport flux further than Q_A^- per RC; ETC – electron transport chain; F_m – maximal (Chl) fluorescence intensity; FNR – ferredoxin-$NADP^+$ reductase; $F_O = F_{0.05ms}$ – minimal (Chl) fluorescence intensity at time 0.05 ms; M_0 – (approximate) initial slope of the fluorescence transient normalised on the maximal variable fluorescence; N – number of Q_A reduction events between time 0 and T_{Fm}; OEC – oxygen-evolving complex, also known as Mn_4CaO_5 cluster; PC – plastocyanin; P-def – phosphorus-deficient plants; PI_{abs} – performance index (potential) for energy conservation from photons absorbed by PSII antenna to the reduction of Q_B; PI_{tot} – performance index for energy conservation from photons absorbed by PSII antenna until the reduction of PSI acceptors; RC – reaction centre; RC/ABS – number of Q_A reducing RCs per PSII antenna chlorophyll; RC/CS_0 – density of active PSII RCs per cross section; RE_0/RC – electron transport flux until PSI acceptors per PSII RC; T_{Fm} – time (in ms) to reach maximal fluorescence; TR_0/RC – trapped energy flux per RC at t = 0; δ_{R0} – efficiency/probability with which an electron from Q_B is transferred until PSI acceptors; Φ_{E0} – quantum yield of electron transport; Φ_{P0} – maximum quantum yield of primary PSII photochemistry; Φ_{R0} – quantum yield of electron transport flux until PSI electron acceptors; ψ_{E0} – efficiency/probability with which an electron trapped in PSII RC is transferred beyond Q_A^-.
Acknowledgements: This work was supported by Warsaw University of Life Sciences WULS-SGGW (grant number 505-10-010200-M00261-99).

fertilisers, is a nonrenewable resource, sustainable use of phosphorus in agriculture is a necessity (Frydenvang *et al.* 2015).

Phosphate is a phloem-mobile nutrient that plays several key roles in plants: as a structural component of nucleic acids, nucleotides, phosphoproteins, phospholipids (a major component of all cell membranes), and enzyme cofactors, which take part in the regulation of metabolism (Malhotra *et al.* 2018). Both inorganic and organic phosphates in plants serve as buffers in the maintenance of cellular pH. Inorganic phosphate (Pi) is able to form water-stable anhydrides and esters, such as ADP (adenosine diphosphate) and ATP (adenosine triphosphate), which are used for energy storage and transfer in plant biochemical processes.

Addition of phosphate to ADP to form ATP, an energy-transforming process, is known as phosphorylation (*see e.g.*, Sanchez 2006), which is catalysed by ATP synthase. ATP synthase uses the energy from transmembrane proton gradient produced by electron transport chain (ETC) of the 'light-dependent phase of photosynthesis' (*see e.g.*, Junge and Nelson 2015). Proton gradient across thylakoid membrane, which is the accumulation of H^+ in thylakoid lumen and the decrease of H^+ in the chloroplast stroma, results from both noncyclic and cyclic electron flow.

Noncyclic photophosphorylation occurs in thylakoid membranes along with electron transport from water molecule to $NADP^+$. In this two-stage process both PSI and PSII are involved (Govindjee *et al.* 2017; for PSI, *see* Nelson and Yocum 2006; and for PSII, *see* Umena *et al.* 2011). First, the photosynthetic active radiation (PAR) is absorbed in light-harvesting complexes (LHCs), and the absorbed energy is transferred to reaction centres (RCs) of PSI and PSII in the form of excitons. After an exciton reaches the PSII RC, it excites an intrinsic Chl molecule (P_{680}) causing it to transfer an electron to other PSII core components: first pheophytin, then plastoquinone Q_A, and ultimately to plastoquinone Q_B (*see e.g.*, Mirkovic *et al.* 2017). Meanwhile, the Chl molecule in PSII RC returns to the neutral state by receiving an electron from oxygen-evolving complex (OEC), which acquires electrons from water molecules, and, in the process, releases oxygen. Plastoquinone Q_B gains two electrons (Q_B^{2-}), and becomes Q_BH_2, a mobile component, after receiving two protons (H^+), one from a nearby amino acid and one from a bicarbonate ion (*see* Shevela *et al.* 2012). This starts a cascade of consecutive oxidation-reduction reactions *via* the plastoquinone pool to a transmembrane protein cytochrome (cyt) b_6f (*see* Cramer and Kallas 2016). Electrons are then transferred to plastocyanin (PC) which then moves to the inner side of the thylakoid membrane, delivering an electron to oxidized P_{700} (RC of PSI), formed by 'light reaction' in PSI. Oxidized P_{700} is formed through several steps, which start from light absorption by pigments in LHCI antenna. After that, the excitation energy is transferred to PSI RC, and then, through a series of carriers, to a protein binding Fe-S centres and to ferredoxin, a partly mobile Fe-S-cluster, located on the stromal side of the thylakoid membrane. Finally, in the last step of the pathway, FNR catalyses the transfer of electrons to $NADP^+$ forming NADPH. This NADPH, together with ATP, is used in the Calvin-Benson cycle to produce sugars from CO_2 (Roháček *et al.* 2008, Govindjee *et al.* 2017, Shevela *et al.* 2019).

Cyclic photophosphorylation dominates in case of increased demand for ATP over NADPH. It occurs in stroma lamellae, involving only PSI, and results in producing ATP. In this type of photophosphorylation, the electrons released from PSI RC follow a cyclic pathway through a series of carriers on the PSI acceptor side to ferredoxin. From here, alternatively to being used to reduce $NADP^+$ (using FNR), electrons are transported back to the cyt b_6f. Next, the electrons are carried back to the PSI acceptor side involving PC, as described earlier. This pathway also produces a proton-motive force which pumps H^+ across the thylakoid membrane. Finally, this proton concentration gradient is used to power the formation of ATP, using ATP synthase (Logan 2005, Roháček *et al.* 2008).

Phosphorus deficiency has been proven to affect the quantum and carboxylation efficiencies of photosynthesis, content and activity of ribulose-1,5-bisphosphate carboxylase/oxygenase (Rubisco) as well as the regeneration capacity of the primary CO_2 acceptor – ribulose 1,5-biphosphate, RuBP (Fredeen *et al.* 1990, Ripley *et al.* 2004, Lin *et al.* 2009). Weng *et al*. (2008) reported that in P-def rice the electron transport rate was dramatically reduced and suggested that the water-water cycle was used as an efficient electron sink for excessive excitation energy.

Literature findings on P-deficiency effect on photosynthetic electron transport rates are often contradictory. According to Abadia *et al.* (1987), low P supply had no major effect neither on the structure nor on the photosynthetic quantum yield of sugar beet leaves. In their studies on P-def sunflower and maize, Jacob and Lawlor (1993) could not confirm *in vivo* limitation of photosynthetic ETC. On the other hand, in phosphorus-deficient citrus, a decrease in maximum quantum yield of primary PSII photochemistry as well as on the electron transport rate was observed (Guo *et al.* 2002). Ripley *et al.* (2004) reported that P-def *Sorghum* showed decreases in quantum yields of PSII primary photochemistry and ETC, efficiency of ETC beyond plastoquinone Q_A, and in the number of active (Q_A reducing) RCs per PSII chlorophyll antenna molecule. Further, Frydenvang *et al.* (2015) have observed a significant alteration in the OJIP Chl *a* fluorescence transient: the 'disappearance' of the I-step; they have identified the 'fingerprint' of P deficiency associated with the electron transport of photosynthesis in barley. The above findings suggest that further research on this other plants could be very valuable in agronomy.

Diagnosing phosphorus deficiency in plants is very difficult for many reasons. One of them is that the response of crops to phosphorus has been poorly correlated with the total amount of phosphorus in the soil. Moreover, phosphorus-deficient (P-def) plants rarely exhibit the visible foliar symptoms and once they appear, they tend to overlap with other nutrient-deficiency symptoms. Thus, accurate diagnosis requires chemical analysis of plants

to learn about the content of phosphorus in their tissues (Malhotra *et al.* 2018), which is invasive, expensive, and time-consuming. Consequently, there is a demand for a quick, cheap and noninvasive method/tool that could be used for assessing plant phosphorus status on-site. Frydenvang *et al.* (2015) have suggested an analytical method based on Chl fluorescence measurements, and the analysis of the OJIP transients (for a background, *see* Strasser *et al.* 2004, Stirbet and Govindjee 2012).

In this work, a combination of various techniques and tools that allow analysing the changes in structure and performance of photosynthetic apparatus of radish plant was applied to get better understanding of the impairment of photosynthesis due to phosphorus deficiency. Moreover, to find out a specific physiological bioindicator/s that can serve for early detection of phosphorus deficiency in radish plants.

Materials and methods

Plant material and growth conditions: Two radish hybrid cultivars *Raphanus sativus* var. *sativus* 'Suntella F1' (Suntella) and 'Fluo HF1' (Fluo) were grown in a plant growth chamber under a set of controlled conditions, close to optimal for both cultivars. The photoperiod was 14 h in a 24-h cycle; day/night air temperature was 18/13°C, respectively; PPFD was about 250 μmol(photon) m^{-2} s^{-1}; 24-h average relative air humidity was about 50%. Plants were grown in hydroponics with a polyethylene pellets (PE) made from a synthetic resin used as a growth medium. The PE is characterized by a low ion absorption capacity as compared to mineral substrates commonly used as growth media for hydroponics (Prof. Hazem M. Kalaji team invention).

Plants were germinated and kept for the first 6 d on tap water. After that time, the control solution (optimal nutrients content) was applied; these conditions were maintained until the first pair of leaves was fully expanded. Plants were subjected to the stress conditions, *i.e.*, P deficiency on the 16th d of vegetation; thus, the 17th d of vegetation was the 1st d after treatment (1 DAT). Phosphorus deficiency was maintained for 13 d, and then the control conditions were restored (recovery phase). The experiment lasted till the 43rd d of vegetation, *i.e.*, 27 DAT.

Both experimental and control solutions were developed based on the Hoagland solution (Hoagland and Arnon 1950). The control medium contained the following macronutrients (concentration expressed in mmol L^{-1}): N (as NO_3) – 11.63; P (as PO_4) – 1.00; K – 6.50; Ca – 4.00; Mg – 2.00; Na – 1.13; S (as SO_4) – 3.13; Cl – 1.00; while the experimental solution: N (as NO_3) – 14.51; N (as NH_4) – 1.00; P (as PO_4) – 0.00; K – 6.50; Ca – 4.50; Mg – 2.00; Na – 0.00; S (as SO_4) – 2.00; Cl – 2.00. Both the control and the P-deficient solutions contained the same concentration of micronutrients (in μmol L^{-1}): Fe – 118.48; B – 48.57; Cu – 1.60; Zn – 0.97; Mn – 6.51; and Mo – 0.52. For details, *see* Tables 1S and 2S (*supplement*). All the experiments had three replicates.

Measuring methods and devices: Leaf mass (excluding cotyledons) was evaluated five times during the vegetative period, *i.e.*, at 3, 6, 12, 19, and 25 DAT. There were 3 to 27 randomly selected plants harvested for evaluation in each term per each cultivar and treatment. The dry matter content was determined by drying the foliage, then reweighing and expressed as percentage of the fresh mass. Collected foliage was further analysed in order to determine its quantitative content of selected elements: N by high-temperature combustion detection (TCD, *Vario Max CN Element Analyzer*, *Elementar Analysensysteme GmbH*, Germany), while P, K, Mg, S, and Fe by inductively coupled plasma atomic emission spectroscopy (ICP-AES, *Thermo Scientific iCAP 6000*, *Thermo Fisher Scientific Inc.*, USA), after mineralization in 65% HNO_3 and 70% $HClO_4$ (HNO_3:$HClO_4$ = 4:1). Analyses were performed on samples pooled from 3–27 randomly selected plants per each term, cultivar, and treatment.

Gas-exchange parameters: net photosynthetic rate (P_N), transpiration rate (E), stomatal conductance (g_s), and intercellular CO_2 concentration (C_i) were evaluated *in vivo* using an infra-red gas analyser, *LCpro+* (*ADC BioScientific Ltd.*, UK). Measurements were conducted four times during the vegetative period, on 5, 10, 17, and 27 DAT. Measurements were conducted on four fully expanded leaves from the second pair of leaves from randomly selected plants of each cultivar and treatment. Measurements were conducted under ambient light in the growth chamber [PAR = 250 μmol(photon) m^{-2} s^{-1}] and CO_2 concentration *ca*. 400 ppm. Samples were closed in the chamber prior measurement start (settling time) for 5 min.

Microscopy imaging of the structure of palisade mesophyll chloroplasts in leaves of the control as well as phosphorus deficient (P-def) plants was performed using *Leica TCS SP5II* confocal laser scanning microscope (*Leica Microsystems CMS*, Wetzlar, Germany) equipped with a 63× lens (*HCX PLAPO Lambda blue 63*). Two fully expanded leaves, from the middle and the bottom of a leaf rosette (young and old leaves, respectively) of each cultivar, were randomly selected for the experiment; leaves were collected on 11 DAT (cv. Suntella) and 12 DAT (cv. Fluo). Imaging of Chl fluorescence in chloroplasts was performed using fresh hand-made cross sections of a leaf blade embedded in distilled water. Chl fluorescence was excited at 633 nm (He:Ne laser) and recorded from 660 to 705 nm, at a room temperature. The pinhole was set to 1 AU (Airy Unit) to compromise between the brightness of fluorescence signal and the resolution of the image. Twenty-six images were acquired at intervals 0.18 μm along the *z*-axis to visualize grana structures and measure the intensity of Chl fluorescence. Brightly fluorescent discs visible on 2D images were recognized as grana optical cross sections. The height of grana was estimated by the measurement of Chl fluorescence intensity in the central part of grana discs using *z*-stacks of 26 optical sections. Raw data were processed identically between the samples, using *Leica SP5II* software. Image series were 3D-deconvoluted to remove the background and ensure a substantial improvement of the image quality. 3D-reconstruction of grana was performed using *ImageJ*/*Fiji 3D* viewer software (Schindelin *et al.* 2012).

Prompt fluorescence (PF) was recorded using *Handy*

PEA fluorometer (*Hansatech Instruments Ltd.*, Norfolk, UK). Measurements were made *in vivo* on leaves of different ages: leaves from the first pair (old leaves) which were marked with a water-based pen prior to introducing stress conditions and leaves from the second pair, which developed on the prior-marked plants during the vegetative growth (young leaves). Measurement protocol of PF was based on the followings components: one flash of 2,500 μmol(photon) m^{-2} s^{-1} for 1 s duration (gain equal to 1.0). Measurements were conducted in the middle part of a leaf blade after 30 min of dark adaptation. Mean values were derived from 15–37 measurements per treatment at each term per each cultivar.

Data from PF measurements were used in JIP-test analysis. Seventeen biophysical parameters (*see* Cetner *et al.* 2017 for definitions and the formulae used; *cf.* Strasser *et al.* 2004) were selected to quantify PSII behaviour: minimal and maximal fluorescence intensities $F_O = F_{0.05ms}$ and F_m; time (in ms) to reach maximal fluorescence – T_{Fm}; approximate initial slope of the fluorescence transient normalised on the maximal variable fluorescence – M_0; number of Q_A reduction events between time zero (0) and T_{Fm} – N; maximum quantum yield of primary PSII photochemistry – Φ_{P0}; quantum yield of electron transport – Φ_{E0}; quantum yield of electron transport flux until PSI electron acceptors – Φ_{R0}; efficiency/probability with which an electron trapped in PSII RC is transferred beyond Q_A^- – ψ_{E0}; efficiency/probability with which an electron from Q_B is transferred until PSI acceptors – δ_{R0}; number of Q_A reducing RCs per PSII antenna chlorophyll RC/ABS; trapped energy flux per RC at t = 0 – TR_0/RC; electron transport flux further than Q_A^- per RC – ET_0/RC; electron transport flux until PSI acceptors per PSII RC – RE_0/RC; performance indices (potential) for energy conservation from photons absorbed by PSII antenna to the reduction of Q_B – PI_{abs} – and until the reduction of PSI acceptors – PI_{tot}; and density of active PSII RCs per cross section – RC/CS_0.

Statistics: Formulas used for calculations of the JIP-test parameters have been presented elsewhere (Cetner *et al.* 2017; *cf.* Strasser *et al.* 2004). The number of repetitions is indicated for each of the performed measurements, and the means and calculated standard error of mean (SEM) are also reported. Analyses were performed using *R software* (*RStudio*, USA) and/or *Microsoft Excel* (*Microsoft*, USA). The significance of difference is presented based on All Pairwise Multiple Comparison Procedures (*Holm-Sidak* method).

Results

Foliar chemical composition: Total phosphorus concentration in plant tissue ranges from ~ 0.1 to 1% (Sanchez 2006). In the foliage of both the cultivars used in this experiment and subjected to phosphorus deficiency, a decrease in total P amount was observed, with the lowest value of 0.97 g kg^{-1} (Fluo) and of 1.05 g kg^{-1} (Suntella) on 12 DAT (Table 3S, *supplement*). Although P concentration was lower in the stressed plants as compared to the control plants, it remained within the above mentioned optimal range during the stress conditions. After the control medium was restored (recovery phase), a 'luxury' uptake of P was observed; its concentration in the foliage of stressed plants of both the cultivars was higher as compared to control plants. Moreover, in the case of cv. Suntella, P concentration reached the highest value on 19 DAT (6^{th} d of recovery).

The optimum range for the total nitrogen concentration in the foliage is considered as > 3–6% (Barker and Bryson 2006). We did not observe any values below the optimum range. The nitrogen concentration in the foliage, regardless of the treatment or cultivar, was more often observed to exceed the optimum range and high of 7.14 and 7.18% in control and P-def plants of cv. Suntella on 3 DAT (Table 3S). (For details on the foliar chemical composition, including K, Mg, S, and Fe, *see* Table 3S)

Foliage morphology, growth, and yield: Phosphorus deficiency symptoms, including the purpling of petioles, and the appearance of pale or chlorotic spots on the older leaves and/or cotyledons, began showing at 7 DAT. At this time, however, deficiency symptoms were not visible. The stunted growth became noticeable only at 12 DAT. During the stress period, the symptoms of P deficiency were noticable only if compared directly to the control plants of the same age for the individual cultivar. After resorting the growth medium to optimal nutritional conditions (as in the control treatment), P-def plants of both cultivars showed an increase in their growth (Fig. 1*A*,*B*). The foliage yield of P-def plants remained lower as compared to the control plants by the end of the vegetative period.

Interestingly, the dry matter production was slightly higher in the P-def plants of both the cultivars, with a significant difference on 3 DAT in case of cv. Suntella (Fig. 1*D*) and on 6 and 12 DAT in the case of cv. Fluo (Fig. 1*C*). In both the control and the P-def plants of both the cultivars, we observed a decreasing tendency in the dry matter production until the end of the vegetative period.

Plant gas-exchange parameters: Net photosynthetic rate (P_N) evaluated for control plants of cv. Fluo was relatively stable, around 9.4 μmol(CO_2) m^{-2} s^{-1}, for most of the vegetative period (data not shown). On the 43^{rd} d of vegetation (27 DAT), a significant decrease was observed, most likely due to the leaf senescence. In the case of P-def plants of cv. Fluo, P_N at 5 DAT remained at the level of the control sample, and a significant decrease was observed on 10 DAT (Fig. 2*A*). After the control medium was restored, the P_N recovered up to the level of the control sample, but decreased again by the end of the vegetative period, to a higher extent as compared to control plants. Stomatal conductance (g_s) in P-def plants of cv. Fluo on 5 DAT remained at the level of the control sample (data not shown), but a significant decrease was observed on 10 DAT (Fig. 2*A*). After the control medium was restored, g_s on 17 DAT increased and extended g_s recorded in the control plants (data not shown). Transpiration rate (E) of the P-def plants was lower than that in the control plants during the stress period, but it increased after the control medium was restored, exceeding the E of the control

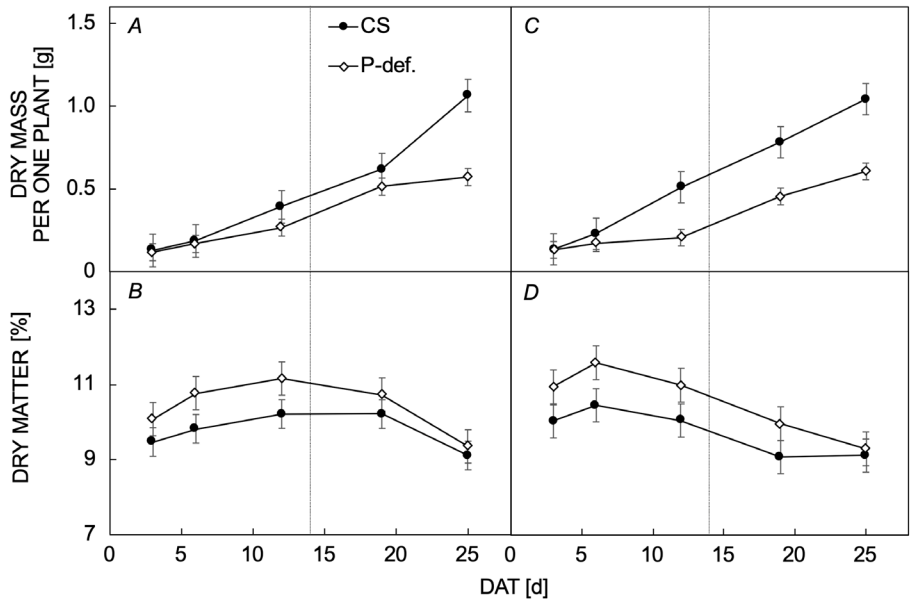

Fig. 1. Dynamics of changes in the dry mass of foliage per plant (*A*,*C*) and the dry matter content (*B*,*D*) in control (CS) and phosphorus deficient (P-def) plants of two *Raphanus sativus* var. *sativus* cultivars 'Fluo HF1' (*A*,*B*) and 'Suntella F1' (*C*,*D*) during the vegetative period. Mean values (± SEM) were derived from 3–27 plants per treatment. *Vertical dotted line* indicates the start of the recovery period on the 14th d after treatment (DAT).

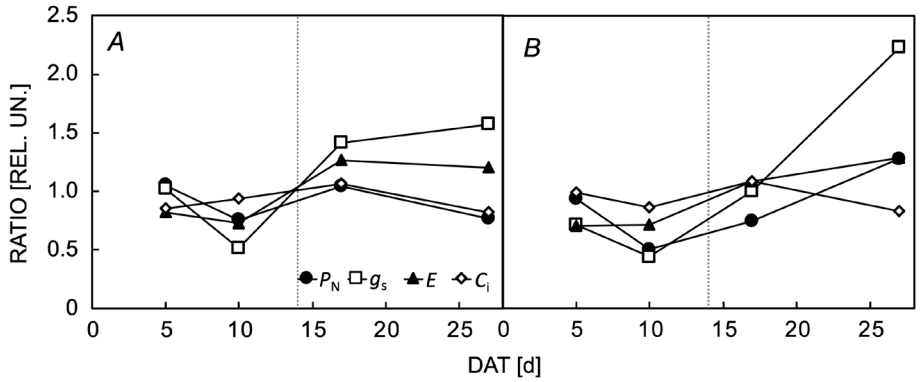

Fig. 2. Gas-exchange parameters presented as a ratio of the control sample: net photosynthetic rate (P_N), transpiration rate (E), stomatal conductance (g_s), and intercellular CO_2 concentration (C_i) in leaves of two *Raphanus sativus* L. var. *sativus* cultivars: 'Fluo HF1' (*A*) and 'Suntella F1' (*B*). Mean values were derived from four measurements per treatment. *Vertical dotted line* shows the start of the recovery period on the 14th d after treatment (DAT).

plants (Fig. 2*A*). Intercellular CO_2 concentration (C_i) significantly decreased in P-def plants of cv. Fluo during the stress period and by the end of vegetative period, that is on 27 DAT (Fig. 2*A*).

In the case of cv. Suntella, P_N of the control plants was 9.8 μmol(CO_2) m^{-2} s^{-1} (on average), with a peak of 12.5 μmol(CO_2) m^{-2} s^{-1} on the 33rd d of vegetation (17 DAT), but then there was a slight decrease by the end of vegetative period (data not shown). P-def plants of cv. Suntella had the P_N at the level of the control plants on 5 DAT, but a significant decrease was observed on 14 DAT (Fig. 2*B*). After the control medium was restored, the P_N of P-def plants recovered to the initial level of 9.8 μmol(CO_2) m^{-2} s^{-1} (data not shown). The g_s in P-def plants, during stress period, was slightly lower than that in the control plants; however, the difference was not significant at the α=0.05 (data not shown). A significant increase was observed by the end of the recovery period, when the g_s of the P-def plants exceeded those of the control plants more than twice (data not shown). The E in P-def plants remained lower as compared to that in the control plants during the stress period; it recovered to the level of control plants after the control medium was restored, and increased by the end of vegetative period (Fig. 2*B*). The C_i in the P-def plants remained at a relatively stable level of 410 ppm during the vegetative period (data not shown). The significant decrease in C_i value on 27 DAT (Fig. 2*B*) resulted from the increase to 508 ppm observed in the control sample (data not shown).

Confocal laser scanning microscopy imaging (CLSM): CLSM sectioning in the *z*-axis revealed brightly fluorescent red discs in the chloroplasts of the two radish cultivars Suntella and Fluo, used here. These discs represent optical sections through thylakoid grana network since at room temperature only Chl fluorescence from PSII, located mainly in the grana, can be detected. Both 2D-images and 3D-reconstructions (Fig 3, *left* and *middle columns*,

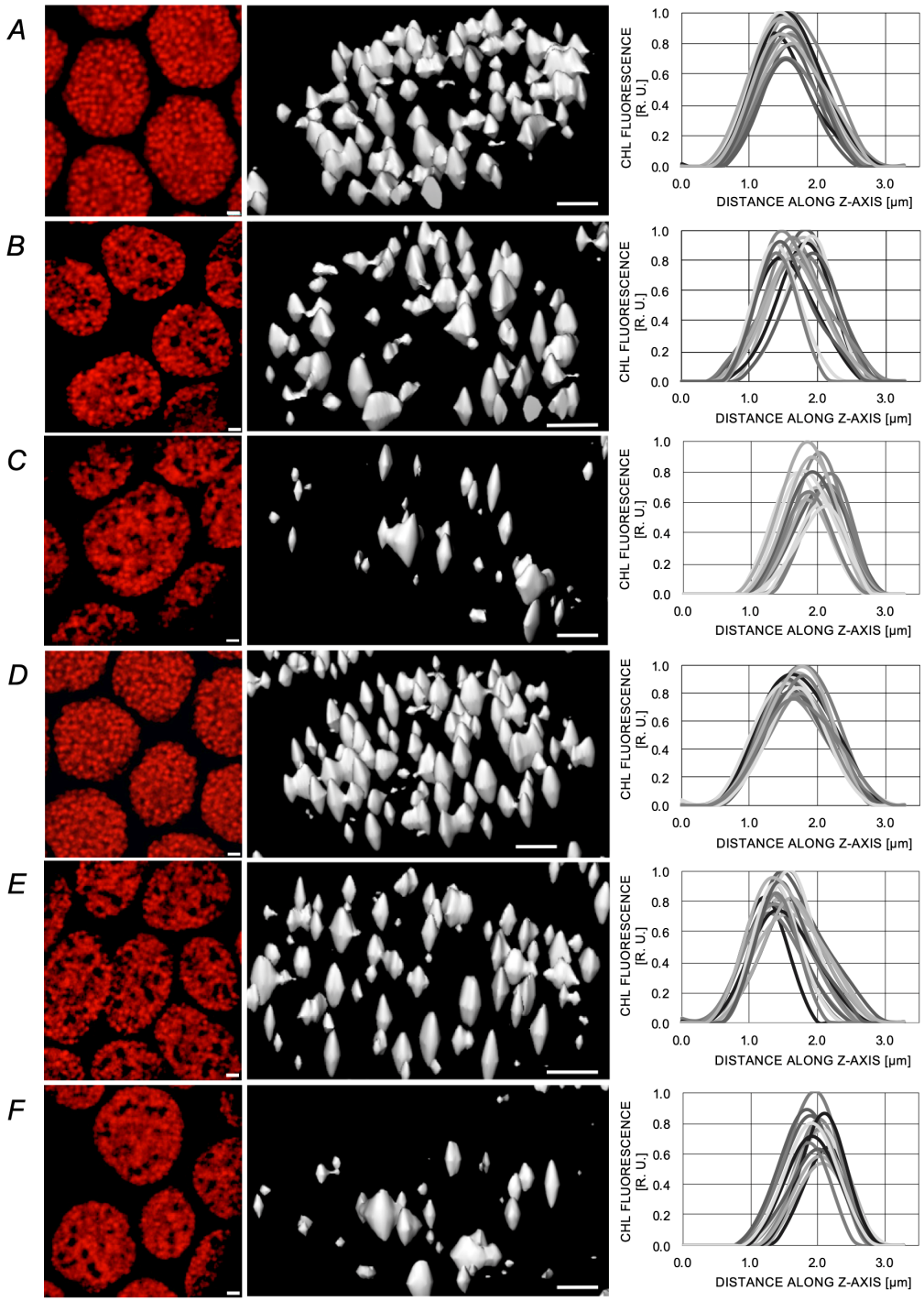

Fig. 3. Comparative data concerning 2D- and 3D-images of grana structures as well as Chl *a* fluorescence intensity along *z*-axis of grana of control and P-def plants of radish cv. 'Fluo HF1' (*A–C*) and cv. 'Suntella F1' (*D–F*). *Left column*: Confocal 2D-images show the groups of chloroplasts. Red fluorescing discs represent grana structures in chloroplast cross section. Notice that in case of P deficiency (*B*,*C*,*E*,*F*) grana structures are less distinguishable as compared to the control sample (*A*,*D*). In case of phosphorus deficiency (especially severe symptoms), bright fluorescence discs representing grana were not easily distinguishable (*C*,*F*). Scale bars = 1µm. *Middle column*: 3D-reconstructions of grana in chloroplasts of control and P-def plants. We note that under phosphorus deficiency (*B*,*C*,*E*,*F*) grana become loosely arranged within chloroplasts. Severe P deficiency symptoms (*C*,*F*) are characterized by a substantial reduction of grana number per chloroplast. Scale bars = 2µm. *Right column*: Chl fluorescence intensity along *z*-axis of 15 randomly chosen grana stacks of five chloroplasts is presented. We note that grana of P-def plants [especially in the case of severe deficiency (*C*,*F*)] are shorter in size than those of the control sample.

respectively) showed equally distributed grana structures within the chloroplasts of the control plants (Fig 3*A*,*D*). P deficiency in young leaves after 12 DAT in the case of cv. Fluo (Fig 3*B*,*C*) and after 11 DAT in the case of cv. Suntella (Fig. 3*E*,*F*) resulted in the appearance of dark spaces between grana network. Enlargement of the spaces coincided with reduction of grana number per chloroplast. In case of phosphorus deficiency (especially severe symptoms), bright fluorescence discs representing grana were not easily distinguishable (compare confocal images of control and phosphorus deficient chloroplasts, Fig. 3). Three-dimensional reconstructions of grana revealed their uniform distribution within median optical profiles of control chloroplasts. Phosphorus deficiency resulted in a lower number of grana structures as well as the presence of distinct areas within chloroplast profile where no Chl fluorescence was observed. Measurements of Chl *a* fluorescence intensity in the *z*-axis (Fig. 3, *right column*) revealed that thylakoid stacks were smaller in size the P-def plants (mild and severe symptoms ~ 2.0 and 1.75 μm, respectively) as compared to control ones (*ca.* 2.5 μm).

Prompt fluorescence induction curves: Double normalization of Chl *a* fluorescence fast induction curves at F_O and F_m allowed comparing the shapes of the curves recorded for P-def and control plants (Fig. 4). In both cultivars, a distinctive shape alteration was observed: 'disappearance' of the I-step (Fig. 5). The I-step decreased gradually along with the time from the introduction of P deficiency; on 13 DAT the induction curve increased in an almost straight line from the J- to the P-step; after the control solution with optimal nutrient content was restored (recovery period), the I-step reappeared (Figs. 4, 5).

The fading of the I-step was observed regardless of leaf age. However, in the case of cultivar Suntella, there were additional curve alterations observed that were differentiated between old and young leaves (Fig. 4). In the case of old leaves, a slight increase in Chl *a* fluorescence intensity was observed, especially at the initial phase of the curve from F_O to F_J (0.05–2 ms). On the contrary, fluorescence signal recorded in young leaves decreased around the J-step, as compared to that in the control sample.

JIP-test: Recorded Chl *a* fluorescence signals were used to calculate some selected biophysical parameters which quantify the efficiency of electron trapping and transport in photochemical phase of photosynthesis [*see e.g.*, Cetner *et al.* (2017) for the definition of parameters as well as equations used for calculations]. Changes in the values of JIP-test parameters, observed in our experiment, were similar between the two cultivars, although they were much more pronounced in cv. Suntella. In both cultivars, there were differences between the old and the young leaves. This is due that phosphate is a 'phloem mobile' nutrient thus, it is relocated from the older leaves to the area of new growth. Therefore, the old leaves as compared to the young ones, showed much more severe symptoms of P deficiency.

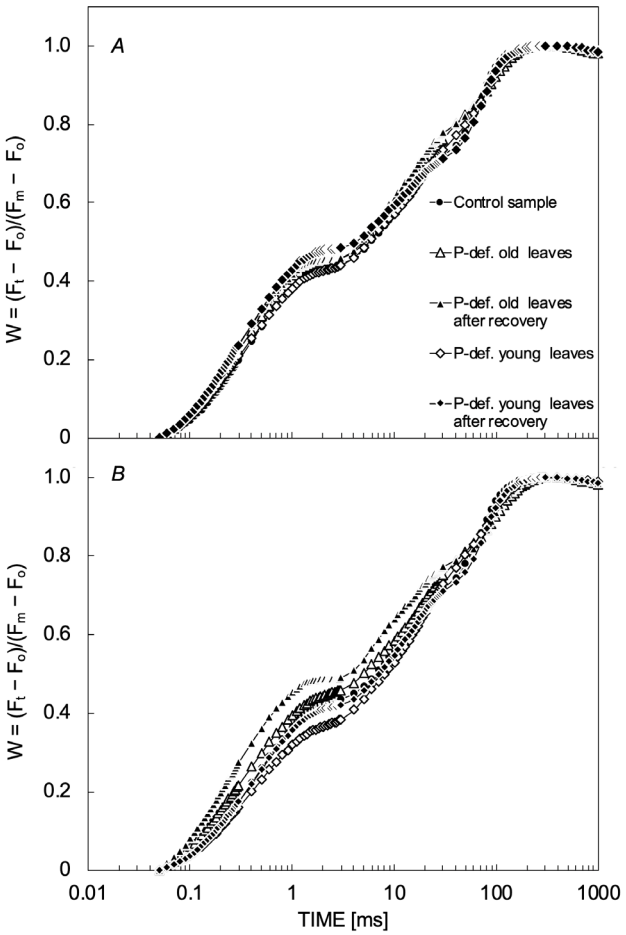

Fig. 4. Changes in the relative shape of chlorophyll *a* fluorescence fast induction curves of dark-adapted leaves of different ages (old, bottom leaves and young, upper leaves) of phosphorus deficient plants (on 13th d after treatment, DAT) and phosphorus deficient plants after recovery (on 27 DAT) of *Raphanus sativus* var. *sativus* cultivars 'Fluo HF1' (*A*) and 'Suntella F1' (*B*) presented as kinetics of relative variable fluorescence $W = (F_t - F_O)/(F_m - F_O)$. Mean values were derived from 15–37 measurements.

The increase in values of several parameters was observed in the old leaves. This included the followings: F_O, which indicates detachment of PSII Chl antenna complexes (LHCII) (Schmidt *et al.* 2016); M_0, net rate of RCs closure; and N, number of Q_A reduction events (Strasser *et al.* 2004). Increases in the last two reflected in increased fluxes of electron trapping (TR_0/RC), electron transport further than Q_A^- (ET_0/RC) and electron transport until PSI acceptors (RE_0/RC) per active PSII RC. Although specific energy fluxes per active RC increased, the quantum yields of PSII primary photochemistry (Φ_{P0}); electron transport (Φ_{E0}); electron transport until PSI acceptors (Φ_{R0}); and efficiency/probability that the electron trapped in PSII RC is transferred beyond Q_A (ψ_{E0}) were reduced. Also, the number of Q_A reducing RCs per PSII Chl antenna (RC/ABS) decreased. As a result, performance indexes for energy conservation from photons absorbed by PSII antenna to the reduction of Q_B (PI_{abs}) and until the reduction of PSI acceptors (PI_{tot}) were reduced. The

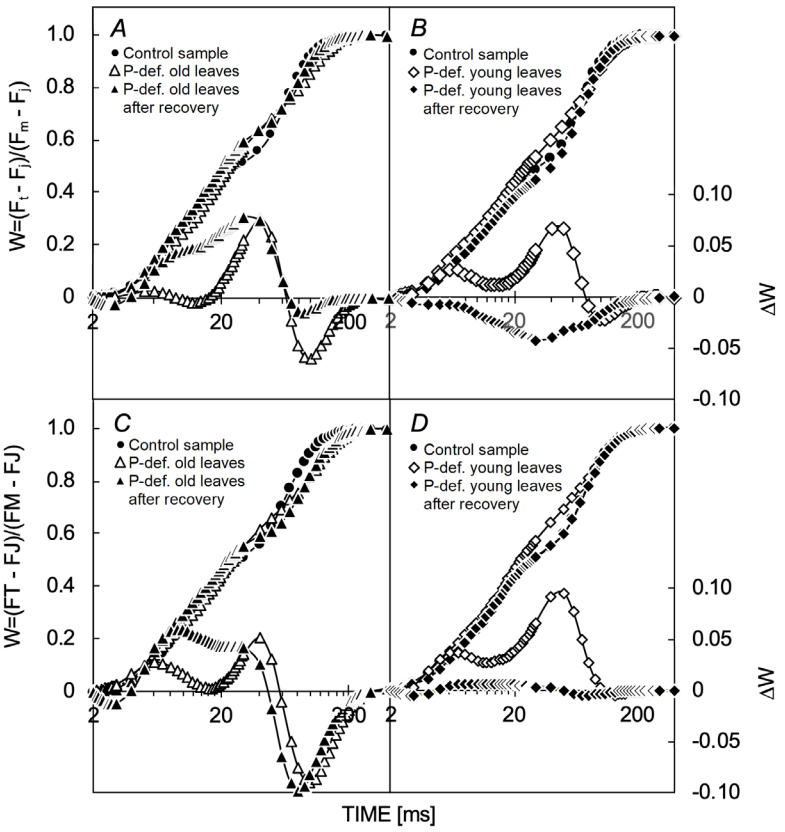

Fig. 5. Changes in the relative shape of chlorophyll *a* fluorescence fast induction curves of dark-adapted leaves of different ages [old, bottom leaves (*A*,*C*) and young, upper leaves (*B*,*D*)] of phosphorus-deficient plants on 13th d of treatment (DAT) and phosphorus-deficient plants after recovery (on 27 DAT) of *Raphanus sativus* var. *sativus* cultivars 'Fluo HF1' (*A*,*B*) and 'Suntella F1' (*C*,*D*) presented as kinetics of relative variable fluorescence $W = (F_t - F_j)/(F_m - F_j)$ (*left axis*) and as difference kinetics ΔW between phosphorus-deficient and control plants (*right axis*). Mean values were derived from 15–37 measurements.

parameter describing efficiency/probability with which an electron from Q_B is transferred until PSI acceptors (δ_{R0}) remained unaffected (Table 1, Fig. 1S, *supplement*).

Increases in both F_O and F_m parameters were observed in young leaves (Table 1, Fig. 1S). In cv. Fluo, density of active PSII RCs per cross section CS (RC/CS_0) also increased. In young leaves of both the cultivars, as in the case of old leaves, specific energy fluxes per active PSII RC (TR_0/RC, ET_0/RC, RE_0/RC) increased, and the number of Q_A reducing RCs per PSII Chl antenna (RC/ABS) decreased. On the contrary, the quantum yield parameters (Φ_{P0}, Φ_{E0}, Φ_{R0}) remained unaffected, although there was observed an increase in efficiency/probability that the electron trapped in PSII RC is transferred beyond Q_A (ψ_{E0}) along with a decrease in efficiency/probability with which an electron from Q_B is transferred until PSI acceptors (δ_{R0}). Therefore, PI_{tot} was reduced, but no change was observed in PI_{abs}.

Increases in specific energy fluxes (per active RC) were due to the decrease in the number of active (Q_A reducing) RCs. Overall quantum yields and efficiency of energy conservation decreased, which is in agreement with the results of Ripley *et al.* (2004).

Discussion

In this study conducted on two radish cultivars, we focused on the response of the photosynthetic apparatus to phosphorus deficiency-induced stress. Our results showed that P deficiency affected several features, including plant morphology, structure of the chloroplasts, the rate of photosynthesis, as well as the quantum yield and the efficiency of electron transport. We also found that the effect of P deficiency on photosynthesis can be reversible if the plants are supplied again with an optimal dose of phosphate; this finding is in agreement with the observations of Frydenvang *et al.* (2015) on other plants.

Decreases in the P_N as well as in g_s (Fig. 2) indicate that stomatal limitation may be partially responsible for the decrease in photosynthesis (Weng *et al.* 2008). However, the relatively steady level of C_i suggests that a nonstomatal factor can be the primary cause of decreased CO_2 assimilation in P-def plants (Lin *et al.* 2009). Weng *et al.* (2008) suggested that the decline in P_N might be due to the slow-down of photosynthetic carbon reduction cycle under P deficiency.

The observed changes in chloroplasts ultrastructure by the confocal laser scanning microscopy imaging, *i.e.*, reduction of grana number per chloroplast and thylakoid membrane systems can be also a reason behind lowering net photosynthetic rate, plants photosynthetic efficiency under stress conditions, and changes in the shape of Chl fluorescence induction curves (Zhang *et al.* 2010).

The analysis of Chl fluorescence parameters allowed us to probe the PSII activity and electrons transfer in the light-dependent phase of photosynthesis (Strasser *et al.* 2004, Joly *et al.* 2010). In our research, we observed a flattened I-step at the time of 30 ms (Figs. 4, 5). A similar finding has been reported by Frydenvang *et al.* (2015) in barley. This confirms this trait of Chl *a* fluorescence

Table 1. Effect of P deficiency (13 DAT) on *Raphanus sativus* var. *sativus* cv. 'Fluo HF1' and cv. 'Suntella F1' analysed with JIP-test parameters. Means ± SEM were derived from 15 to 37 measurements. The significance of difference is presented based on All Pairwise Multiple Comparison Procedures (*Holm-Sidak* method). Significant difference (α=0.05) is denoted by *; nonsignificant by ^{ns}. CS – control sample, –P – phosphorus deficient plants.

Parameter	Old leaves		Young leaves	
	CS	–P	CS	–P
Fluo HF1				
$F_O = F_{0.05\ ms}$	606.900 ± 48.933	959.125 ± 47.379*	728.815 ± 51.580	953.129 ± 48.137*
F_m	3,100.333 ± 64.146	3,111.094 ± 62.109^{ns}	2,963.185 ± 67.616	3,475.323 ± 63.103*
T_{Fm}	268.000 ± 13.517	259.375 ± 13.088^{ns}	301.852 ± 14.248	281.290 ± 13.297^{ns}
M_0	0.708 ± 0.039	0.941 ± 0.038*	0.846 ± 0.041	0.844 ± 0.039^{ns}
N	19.290 ± 0.796	21.821 ± 0.771^{ns}	21.159 ± 0.839	20.933 ± 0.783^{ns}
Φ_{P0}	0.804 ± 0.018	0.687 ± 0.017*	0.736 ± 0.019	0.728 ± 0.017^{ns}
Φ_{E0}	0.473 ± 0.017	0.377 ± 0.016*	0.386 ± 0.018	0.419 ± 0.016^{ns}
Φ_{R0}	0.209 ± 0.007	0.164 ± 0.007*	0.199 ± 0.008	0.194 ± 0.007^{ns}
ψ_{E0}	0.586 ± 0.014	0.538 ± 0.014*	0.516 ± 0.015	0.570 ± 0.014*
δ_{R0}	0.447 ± 0.016	0.448 ± 0.016^{ns}	0.521 ± 0.017	0.473 ± 0.016*
RC/ABS	0.478 ± 0.014	0.349 ± 0.014*	0.429 ± 0.015	0.382 ± 0.014*
TR_0/RC	1.702 ± 0.036	2.016 ± 0.034*	1.733 ± 0.037	1.940 ± 0.035*
ET_o/RC	0.994 ± 0.023	1.075 ± 0.022*	0.888 ± 0.024	1.096 ± 0.022*
RE_0/RC	0.443 ± 0.016	0.478 ± 0.016^{ns}	0.457 ± 0.017	0.517 ± 0.016*
PI_{abs}	3.040 ± 0.188	1.374 ± 0.182*	1.848 ± 0.198	1.713 ± 0.185^{ns}
PI_{tot}	2.395 ± 0.152	1.007 ± 0.147*	1.963 ± 0.161	1.459 ± 0.150*
RC/CS_0	284.890 ± 6.481	308.949 ± 6.275*	302.340 ± 6.832	342.180 ± 6.376*
Suntella F1				
$F_O = F_{0.05\ ms}$	627.233 ± 37.848	1066.480 ± 41.460*	671.214 ± 39.176	768.577 ± 40.655^{ns}
F_m	3,078.167 ± 53.894	2,699.120 ± 59.038*	3,210.893 ± 55.785	3,502.385 ± 57.891*
T_{Fm}	293.000 ± 11.552	330.400 ± 12.654^{ns}	313.929 ± 11.957	313.077 ± 12.409^{ns}
M_0	0.684 ± 0.035	0.978 ± 0.038*	0.710 ± 0.036	0.643 ± 0.038^{ns}
N	20.244 ± 0.839	26.694 ± 0.919*	21.925 ± 0.868	20.316 ± 0.901^{ns}
Φ_{P0}	0.796 ± 0.017	0.587 ± 0.018*	0.790 ± 0.017	0.779 ± 0.018^{ns}
Φ_{E0}	0.456 ± 0.015	0.322 ± 0.017*	0.442 ± 0.016	0.494 ± 0.016*
Φ_{R0}	0.205 ± 0.006	0.147 ± 0.007*	0.232 ± 0.006	0.212 ± 0.007*
ψ_{E0}	0.571 ± 0.012	0.523 ± 0.013*	0.556 ± 0.012	0.633 ± 0.013*
δ_{R0}	0.454 ± 0.014	0.488 ± 0.015^{ns}	0.536 ± 0.014	0.429 ± 0.015*
RC/ABS	0.510 ± 0.014	0.307 ± 0.015*	0.505 ± 0.014	0.447 ± 0.015*
TR_0/RC	1.583 ± 0.034	2.011 ± 0.037*	1.585 ± 0.035	1.751 ± 0.036*
ET_0/RC	0.899 ± 0.017	1.033 ± 0.018*	0.875 ± 0.017	1.107 ± 0.018*
RE_0/RC	0.404 ± 0.010	0.498 ± 0.011*	0.463 ± 0.010	0.475 ± 0.010^{ns}
PI_{abs}	2.941 ± 0.183	1.006 ± 0.200*	2.718 ± 0.189	2.861 ± 0.196^{ns}
PI_{tot}	2.401 ± 0.154	0.771 ± 0.169*	3.004 ± 0.160	2.177 ± 0.166*
RC/CS_0	312.516 ± 6.170	286.533 ± 6.759*	332.868 ± 6.387	341.205 ± 6.628^{ns}

induction curves as distinguishable in P-def plants and can be used as bioindicator to predict and monitor plant nutrient status. The sigmoidal rise from the step I to P has been suggested to reflect the electron transfer through PSI and the induction of a 'traffic jam' of electrons caused by a block at the PSI acceptor side (*cf.* Munday and Govindjee 1969, Schansker *et al.* 2005, Joly and Carpentier 2007). Schansker *et al.* (2005) observed the disappearance of the I-step after blocking the electron flow towards PSI by dibromothymoquinone (DBMIB), together with creating a 'bypass' of the transient block at the PSI acceptor side by methylviologen (MV) (*cf.* Munday and Govindjee 1969). The artificial quinone DBMIB acts as an inhibitor of ETC and an antagonist of PQ, which binds to the cyt b_6f complex, preventing the reoxidation of other PQH_2 molecules by cyt b_6f and blocking the electron transfer to PSI (Rich *et al.* 1991, Schansker *et al.* 2005). On the other hand, MV acts as an effective electron acceptor which competes strongly with ferredoxin for electrons from the Fe-S cluster of PSI. As a consequence, MV suppresses the cyclic phosphorylation around PSI (Cornic *et al.* 2000, Schansker *et al.* 2005). Considering the above

mentioned findings, the disappearance of the I-step in the case of P-def plants can be connected to the disturbances in ETC beyond PSII and/or the reduction of PSI acceptors (inactivation of PSI and suppression of the cyclic phosphorylation) (*cf.* Joly *et al.* 2010, Frydenvang *et al.* 2015). Furthermore, several studies (*see e.g.*, Hamdani *et al.* 2015) have shown a clear relationship of the slope of the IP phase with photosynthetic performance (and even biomass accumulation); thus, further research is needed on this point in P-deficient (to different degrees) and control as well as recovered plants.

The JIP-test analysis of chlorophyll *a* fluorescence under phosphorus deficiency stress showed the LHCII detachment (increased F_O) and the decrease in active (Q_A reducing) PSII RCs per Chl antenna (RC/ABS), followed by decreases in quantum yields of the primary PSII photochemistry (Φ_{P0}), electron transport (Φ_{E0}) and electron transport until PSI acceptors (Φ_{R0}) along with the efficiency/probability that the electron trapped in PSII RC is transferred beyond Q_A (ψ_{E0}), as the main causes of ETC suppression (Table 1, Fig. 1S). The first two changes, *i.e.*, LHCII uncoupling and inactivation of RCs, are connected with mechanisms protecting PSII against photoinhibition (Roháček *et al.* 2008, Belgio *et al.* 2012, Kalaji *et al.* 2016), hence they can be considered as nonspecific stress indicators.

The primary photochemistry of PSII is partly regulated by electron flow from OEC at the donor side and by the electron flow leaving the RC towards the acceptor side (Strasser *et al.* 2004). The inactivation of OEC could be connected with the appearance of a positive K-band at about 300 μs (Yusuf *et al.* 2010, Stirbet *et al.* 2014, Kalaji *et al.* 2016). Since there was no clear K-band observed in the induction curves revealed for P-def plants (data not shown), we assume that PSII efficiency was suppressed mainly at its acceptor side. Activity of plastoquinones at PSII acceptor side generates the transmembrane pH gradient. At the same time, the reaction between PQH_2 and the Rieske Fe-S protein of the cyt b_6f complex is sensitive to pH. The pH sensitivity of this reaction plays a key role in the regulation of both linear and cyclic ETC (Foyer *et al*. 2012). Hence the limitation of photosynthesis observed in P-def plants may have resulted from the end-product inhibition. A decrease in the supply of Pi from the medium leads to a rapid decrease in stromal Pi, to the point where photophosphorylation may become Pi-limited, decreasing the rate of photosynthesis. Moreover, low stromal Pi concentration has a direct, downregulating effect on Rubisco by various mechanisms (Rychter and Rao 2005).

We conclude that our above discussed findings, as well as our old previous similar ones, could be exploited in discovering sensitive bioindicators for nutrients deficiency in plants. Moreover, since most of JIP-test parameters are connected with mathematical equations, implementing of advanced statistical and modelling procedures, *e.g.*, principal component analysis (PCA) or artificial neural networks (ANN) could be very beneficial for stress identification and 'plant talk' research (Goltsev *et al.* 2012, Kalaji *et al.* 2014, 2017; Frydenvang *et al.* 2015, Cetner *et al.* 2017). This research confirms that in case of some stressors, the alteration of the shape of Chl *a* fluorescence induction curve can serve as a tool for a quick and/or preliminary diagnosis on-site. Disappearance of I-step from the induction curve can be used as a specific physiological bioindicator for early detection of phosphorus deficiency in radish plants.

References

Abadia J., Rao I.M., Terry N.: Changes in leaf phosphate status have only small effects on the photochemical apparatus of sugar beet leaves. – Plant Sci. **50**: 49-55, 1987.

Barker A.V., Bryson G.M.: Nitrogen. – In: Barker A.V., Pilbeam D.J. (ed.): Handbook of Plant Nutrition. Books in Soils, Plants, and the Environment. Vol. 117. Pp. 21-50. CRC Press, Boca Raton 2006.

Belgio E., Johnson M.P., Jurić S., Ruban A.V.: Higher plant photosystem II light-harvesting antenna, not the reaction center, determines the excited-state lifetime – both the maximum and the nonphotochemically quenched. – Biophys. J. **102**: 2761-2771, 2012.

Cetner M.D., Kalaji H.M., Goltsev V. *et al.*: Effects of nitrogen-deficiency on efficiency of light-harvesting apparatus in radish. – Plant Physiol. Bioch. **119**: 81-92, 2017.

Cornic G., Bukhov N.G., Wiese C. *et al*.: Flexible coupling between light-dependent electron and vectorial proton transport in illuminated leaves of C_3 plants. Role of photosystem I-dependent proton pumping. – Planta **210**: 468-477, 2000.

Cramer W.A., Kallas T.: Cytochrome Complexes: Evolution, Structures, Energy Transduction, and Signalling. Pp. 754. Springer, Dordrecht 2016.

Fairhurst T., Lefroy R., Mutert E., Batjes N.: The importance, distribution and causes of phosphorus deficiency as a constraint to crop production in the tropics. – Agrofor. Forum **9**: 2-8, 1999.

Foyer C.H., Neukermans J., Queval G. *et al*.: Photosynthetic control of electron transport and the regulation of gene expression. – J. Exp. Bot. **63**: 1637-1661, 2012.

Fredeen A.L., Raab T.K., Rao I.M., Terry N.: Effects of phosphorous nutrition on photosynthesis of *Glycine max.* (L.) Merr. – Planta **181**: 399-405, 1990.

Frydenvang J., van Maarschalkerweerd M., Carstensen A. *et al.*: Sensitive detection of phosphorus deficiency in plants using chlorophyll *a* fluorescence. – Plant Physiol. **169**: 353-361, 2015.

Goltsev V., Zaharieva I., Chernev P. *et al.*: Drought-induced modifications of photosynthetic electron transport in intact leaves: Analysis and use of neural networks as a tool for a rapid non-invasive estimation. – BBA-Bioenergetics **1817**: 1490-1498, 2012.

Govindjee, Shevela D., Björn L.O.: Evolution of the Z-scheme of photosynthesis: a perspective. – Photosynth. Res. **133**: 5-15, 2017.

Guo Y.P., Chen P.Z., Zhang L.C., Zhang S.L.: [Effects of different phosphorus nutrition levels on photosynthesis in satsuma mandarin (*Citrus unshiu* Marc.) leaves.] – Plant Nutr. Fert. Sci. **8**: 186-191, 2002. [In Chinese]

Hamdani S., Qu M., Xin C.-P. *et al.*: Variations between the photosynthetic properties of elite and landrace Chinese rice cultivars revealed by simultaneous measurements of 820 nm transmission signal and chlorophyll *a* fluorescence induction. – J. Plant Physiol. **177**: 128-138, 2015.

Hoagland D.R., Arnon D.I.: The Water-Culture Method for Growing Plants without Soil. Pp. 32. The College of Agriculture, University of California, Berkeley 1950.

Jacob J., Lawlor D.W.: *In vivo* photosynthetic electron transport does not limit photosynthetic capacity in phosphate-deficient sunflower and maize leaves. – Plant Cell Environ. **6**: 785-795, 1993.

Joly D., Carpentier R.: Regulation of energy dissipation in photosystem I by the redox state of the plastoquinone pool. – Biochemistry-US **46**: 5534-5541, 2007.

Joly D., Jemâa E., Carpentier R.: Redox state of the photosynthetic electron transport chain in wild-type and mutant leaves of *Arabidopsis thaliana*: Impact on photosystem II fluorescence. – J. Photoch. Photobio. B **98**: 180-187, 2010.

Junge W., Nelson N.: ATP synthase. – Annu. Rev. Biochem. **84**: 631-657, 2015.

Kalaji H.M., Jajoo A., Oukarroum A. *et al.*: Chlorophyll *a* fluorescence as a tool to monitor physiological status of plants under abiotic stress conditions. – Acta Physiol. Plant. **38**: 102, 2016.

Kalaji H.M., Schansker G., Brestič M. *et al*.: Frequently asked questions about chlorophyll fluorescence, the sequel. – Photosynth. Res. **132**: 13-66, 2017.

Kalaji H.M., Schansker G., Ladle R.J. *et al*.: Frequently asked questions about *in vivo* chlorophyll fluorescence: practical issues. – Photosynth. Res. **122**: 121-158, 2014.

Lin Z.H., Chen L.S., Chen R.B. *et al.*: CO_2 assimilation, ribulose-1,5-bisphosphate carboxylase/oxygenase, carbohydrates and photosynthetic electron transport probed by the JIP-test, of tea leaves in response to phosphorus supply. – BMC Plant Biol. **9**: 43, 2009.

Logan B.A.: Chlorophyll *a* fluorescence: A signature of photosynthesis. – J. Torrey Bot. Soc. **132**: 650, 2005.

MacDonald G.K., Bennett E.M., Potter P.A., Ramankutty N.: Agronomic phosphorus imbalances across the world's croplands. – P. Natl. Acad. Sci. USA **108**: 3086-3091, 2011.

Malhotra H., Vandana, Sharma S., Pandey R.: Phosphorus nutrition: Plant growth in response to deficiency and excess. – In: Hasanuzzaman M., Fujita M., Oku H. *et al*. (ed.): Plant Nutrients and Abiotic Stress Tolerance. Pp. 171-190. Springer, Singapore 2018.

Mirkovic T., Ostrumov E.E., Anna J.M. *et al*.: Light absorption and energy transfer in the antenna complexes of photosynthetic organisms. – Chem. Rev. **117**: 249-293, 2017.

Munday J.C., Govindjee: Light-induced changes in the fluorescence yield of chlorophyll *a in vivo*. III. The dip and the peak in the fluorescence transient of *Chlorella pyrenoidosa*. IV. The effect of preillumination on the fluorescence transient of *Chlorella pyrenoidosa*. – Biophys. J. **9**: 1-35, 1969.

Nelson N., Yocum C.F.: Structure and function of photosystems I and II. – Annu. Rev. Plant Biol. **57**: 521-565, 2006.

Rich P.R., Madgwick S.A., Moss D.A.: The interactions of duroquinol, DBMIB and NQNO with the chloroplast cytochrome *bf* complex. – BBA-Bioenergetics **1058**: 312-328, 1991.

Ripley B.S., Redfern S.P., Dames J.: Quantification of the photosynthetic performance of phosphorus-deficient *Sorghum* by means of chlorophyll-*a* fluorescence kinetics. – S. Afr. J. Sci. **100**: 615-618, 2004.

Roháček K., Soukupová J., Barták M.: Chlorophyll fluorescence: A wonderful tool to study plant physiology and plant stress. – In: Schoefs B. (ed.): Plant Cell Compartments – Selected Topics. Pp. 41-104. Research Signpost, Kerala 2008.

Rychter A.M., Rao I.M.: Role of phosphorus in photosynthetic carbon metabolism. – In: Pessarakli M. (ed.): Handbook of Photosynthesis. 2nd Edition. Pp. 123-148. Marcel Dekker, Inc., New York 2005.

Sanchez C.A.: Phosphorus. – In: Barker AV, Pilbeam DJ (ed.): Handbook of Plant Nutrition. Books in Soils, Plants, and the Environment. Vol. 117. Pp. 51-90. CRC Press, Boca Raton 2006.

Schansker G., Tóth S.Z., Strasser R.J.: Methylviologen and dibromothymoquinone treatments of pea leaves reveal the role of photosystem I in the Chl *a* fluorescence rise OJIP. – BBA-Bioenergetics **1706**: 250-261, 2005.

Schindelin J., Arganda-Carreras I., Frise E. *et al.*: Fiji: an open-source platform for biological-image analysis. – Nat. Methods **9**: 676-682, 2012.

Schmidt S.B., Powikrowska M., Krogholm K.S. *et al.*: Photosystem II functionality in barley responds dynamically to changes in leaf manganese status. – Front. Plant Sci. **7**: 1772, 2016.

Shevela D., Björn L.O., Govindjee: Photosynthesis: Solar Energy for Life. Pp. 204. World Scientific Publishing, Singapore 2019.

Shevela D., Eaton-Rye J.J., Shen J.-R., Govindjee: Photosystem II and unique role of bicarbonate: A historical perspective. – BBA-Bioenergetics **1817**: 1134-1151, 2012.

Stirbet A., Govindjee: Chlorophyll *a* fluorescence induction: A personal perspective of the thermal phase, the J-I-P rise. – Photosynth. Res. **113**: 15-61, 2012.

Stirbet A., Riznichenko G.Y., Rubin A.B., Govindjee: Modeling Chlorophyll *a* fluorescence transient: Relation to photosynthesis. – Biochemistry-Moscow+ **79**: 291-323, 2014.

Strasser R.J., Tsimilli-Michael M., Srivastava A.: Analysis of the chlorophyll *a* fluorescence transient. – In: Papageorgiou G.C., Govindjee (ed.): Chlorophyll *a* Fluorescence: A Signature of Photosynthesis. Advances in Photosynthesis and Respiration. Pp. 321-362. Springer, Dordrecht 2004.

Umena Y., Kawakami K., Shen J.R., Kamiya N.: Crystal structure of oxygen-evolving photosystem II at 1.9 Å resolution. – Nature **473**: 55-60, 2011.

Weng X.Y., Xu H.X., Yang Y., Peng H.H.: Water-water cycle involved in dissipation of excess photon energy in phosphorus deficient rice leaves. – Biol. Plantarum **52**: 307-313, 2008.

Yusuf M.A., Kumar D., Rajwanshi R. *et al.*: Overexpression of γ-tocopherol methyl transferase gene in transgenic *Brassica juncea* plants alleviates abiotic stress: physiological and chlorophyll *a* fluorescence measurements. – BBA-Bioenergetics **1797**: 1428-1438, 2010.

Zhang M.P., Zhang C.J., Yu G.H. *et al.*: Changes in chloroplast ultrastructure, fatty acid components of thylakoid membrane and chlorophyll *a* fluorescence transient in flag leaves of a super-high-yield hybrid rice and its parents during the reproductive stage. – J. Plant Physiol. **167**: 277-285, 2010.